RSC Advances

ROYAL SOCIETY OF CHEMISTRY

www.rsc.org/advances

Identification and Distinction of Non-small-cell Lung Cancer Cells by Intracellular SERS Nanoprobes

Yuqing Zhang,[a] Xiaojia Ye,[,b] Gengxin Xu,[b] Xiulong Jin,[a] Mengmeng Luan,[b] Jiatao Lou,[c] Lin Wang,[c] Chengjun Huang,[d] and Jian Ye[*,a]*

[a.] School of Biomedical Engineering & Med-X Research Institute, Shanghai Jiao Tong University, 1954 Huashan Road, Shanghai 200030, China

[b.] School of Mathematics and Information Science, Shanghai Lixin University of Commerce, 2800 Wenxiang Road, Shanghai 201620, China

[c.] Department of Laboratory Medicine, Shanghai Chest Hospital, Shanghai Jiao Tong University, Shanghai 200030, China

[d.] Key Laboratory of Microelectronics Devices and Integrated Technology, Institute of Microelectronics of Chinese Academy of Sciences, 3 Bei-Tu-Cheng West Road, Beijing 100029, China

* Corresponding author:

(X.Y.) yxj@lixin.edu.cn; Telephone: (86) 021-67705383;

(J.Y.) yejian78@sjtu.edu.cn; Telephone: (86) 021-62934760;

Key words: Surface-enhanced Raman scattering, non-small cell lung cancer cell, hierarchical cluster analysis, principal component analysis, support vector machines

TOC

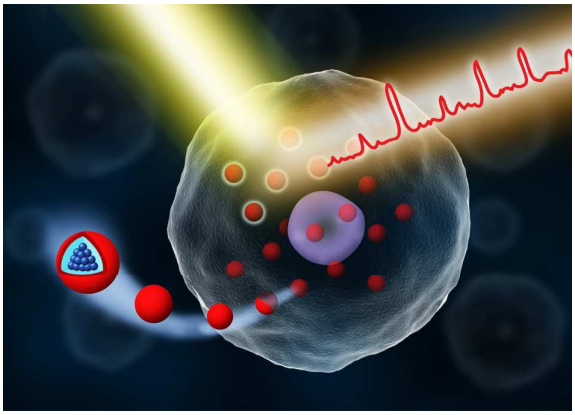

ABSTRACT

Non-small-cell lung cancer (NSCLC) comprises ~75% of all lung cancer and consists of several subtypes. Identification of lung cancer cell subtypes is important for choosing the appropriate therapy plan and reducing the mortality. In this study, we have been able to identify and distinguish three subtypes of NSCLC cells (H1229, H460 and A549) and leukocytes on the single-cell level by combining surface-enhanced Raman scattering (SERS) spectroscopy and multivariate statistical methods. After the evaluation of three statistical methods, support vector machines (SVM) shows the best classification performance compared to hierarchical cluster analysis (HCA) and principal component analysis (PCA) method based on a large amount of cell SERS spectra from Au nanoshells as intracellular nanoprobes. The SVM classification model provides a predication accuracy of 88.75% for "unknown" independent cell types and an accuracy of ~95% for the two subtypes mixed samples on a single-cell level. This method combining SERS and SVM could potentially be adapted to the distinction of other types of cancer cells and be applied for conducting non-invasive downstream cells identification after the captures of circulating tumor cells.

1. Introduction

Lung cancer becomes a leading one of cancer cases worldwide with two main categories: small cell lung cancer (SCLC) and non-small-cell lung cancer (NSCLC).[1] The latter comprises ~75% of all lung cancer and consists of adenocarcinoma, squamous cell carcinoma, large cell carcinoma, and rare types.[2-4] As there is a significant difference in the diagnosis and treatment in each subtype,[5] identification of lung cancer subtypes is important for choosing an appropriate treatment plan, reducing the mortality and increasing the lifetime of patients. Currently, the evaluation of lung cancer subtypes via an invasive procedure that requires tissue specimens is not always feasible, because it is difficult to access the small lung tumor and the sensitivity might be limited due to small tumor size. [6]

At present, there are mainly two types of method to separate and identify cancer cells from blood: one based on physical properties such as size, density and deformability; the other based on biological properties such as protein expressions.[7, 8] However, the methods in the former type including density gradient centrifugation and membrane filtration are difficulty to realize the identification and distinguishing of different types of cancer cells. The methods in the latter type, such as immunomagnetic separation, can only distinguish cancer cells with specific biomarkers and are limited by the spectral overlapping of fluorescent tags.[9] Therefore, the development of new method for the non-invasive, highly sensitive and label-free identification and distinction of closely related cell phenotypes is in urgent need.[10]

Recently, surface-enhanced Raman scattering (SERS) spectroscopy, as a label-free

and ultra-sensitive technique for chemical and biomedical analysis,[11, 12] is emerging as a new powerful tool for the analysis of individual cells, mainly due to its fingerprint spectral characteristic.[10, 13-15] As SERS can enhance the Raman signals of molecules close to metal surface by as much as 6 to 14 orders of magnitude,[16] we can use near-infrared (NIR) light as excitation laser with low laser power and reduced photo-damage to analyze living cells.[17, 18] In SERS, Au nanoparticles are usually used as optical enhancing materials because of their chemical stability, good biocompatibility and strong enhancement capabilities. Au nanoparticles have been employed as intracellular probes facilitating cancer detection in blood plasma,[19, 20] cells,[21, 22] and tissues.[23, 24]

The SERS spectra of cells are derived from cells themselves and no external label is required.[25] SERS spectra of cells can be very complicated, containing spectral information from numerous biological molecules.[26] Various types of cells have different SERS spectra due to their different biomolecular composition and structure, thus it can be used as the basis for distinguishing at a single-cell level.[27, 28] Since the spectral differences are often minute and difficult to identify, multivariate statistical methods such as principal component analysis (PCA) and hierarchical cluster analysis (HCA), have been applied to extract characteristic biochemical information presented in the spectra of different types of cells.[10, 15, 28-31] However, few studies were reported about the application of Au nanoparticles as intracellular SERS probes with multivariate statistical methods for the identification and distinction of NSCLC cells with different subtypes.

In this study, the superparamagnetic Au nanoshells with strong NIR SERS effect were used as intracellular SERS nanoprobes, so that we can get strong signals from cells with lower laser power and less photo-damage. We combine SERS spectroscopy and multivariate statistical methods including HCA, PCA and support vector machines (SVM) to identify and distinguish three closely related NSCLC cell types (A549, H1299 and H460) and leukocytes. We have shown successful segregation of different types of cells using SVM analysis at a single-cell level, while HCA and PCA approach are more difficult to realize. A SVM classification model was built and tested for four independent cell types and mixture samples (two subtypes of NSCLC). The high prediction accuracies indicate that SERS spectra in combination with the SVM method can be a highly sensitive method for the distinction of NSCLC cells with different subtypes. Furthermore, if this method is combined with bio-chips, it will have potential to capture, detect and classify circulating tumor cells.

2. Materials and methods

2.1 Cell culture and sample preparation

The human NSCLC cell lines H1229, H460 and A549 were obtained from American Type Culture Collection (ATCC), and all reagents for the cell culture were purchased from Gibco. The cells were cultured in RPMI 1640 medium supplemented with 10% fetal bovine serum, 100 U/mL penicillin, and 100 μg/mL streptomycin at 37°C in a humidified atmosphere containing 5% CO_2. For Raman measurement purposes, the cells were grown on quartz coverslips to 80% confluence, and then incubated with Au nanoshells (Fe_3O_4@SiO_2@Au) with a final concentration of 0.02 nM for six hours.

The quartz coverslips were pretreated with 75% ethanol and then washed with sterile water, and Au nanoshells were just washed with sterile water before the incubation with cells. Fe_3O_4@SiO_2@Au nanoparticles were synthesized with an average diameter of 180 nm and the detailed procedure was described in our previously published work.[32] We separated leukocytes from peripheral blood of healthy donors following erythrocytes lysis as published before.[33] Since the isolated leukocytes can't be cultured or adhere to the coverslips, the leukocytes suspensions were incubated with Au nanoshell particles with a final concentration of 0.02 nM for six hours.[32]

Following the incubation, the cultured cells and leukocytes were washed extensively with phosphate buffered saline (PBS) and fixed with 4% paraformaldehyde for 10 min at room temperature. Then the excess paraformaldehyde was removed by deionized water. The leukocytes were transferred to quartz coverslips and air-dried together with other cultured cells for SERS measurements. For the mixed cell experiments, A549 were pre-incubated with Au nanoshells, then they were trypsinized and separated by an external magnetic field (Magical Trapper, Toyobo, nearly 200 mT) for 2 min after excess Au nanoshells were removed. For Raman experiments, the Au nanoshells labeled A549 were mixed with blank H1299 at two different ratios of 1:1 and 1:9; then they were cultured on the coverslips and fixed with 4% paraformaldehyde.

2.2 SERS measurement

Raman spectrometer (SR-500, Andor, Northern Ireland) with 785 nm single mode diode laser (Innovative Photonic Solutions, America) was used to collect SERS spectra from the fixed cells on quartz coverslips. The laser power was 4.5 mW on the

sample with a 50x/NA 0.5 objective (Leica, Germany). The scattered Raman signal was detected on a peltier-cooled, back-illuminated, deep-depletion CCD detector (Andor, Northern Ireland). Raman spectra of all individual cells were recorded over a spectra range of 550-1800 cm^{-1}. For each Raman spectrum the collection time was 3 s. For all cells, three Raman spectra were obtained from three different parts of each cell and then averaged.

2.3 Data processing and Analysis

Spectral data from our experiments were pre-processed and analyzed using MATLAB R2011b, Statistical analysis system (SAS), and R-Programme. For all analytical methods, the averaged Raman spectra from each individual cell were used. Statistical analysis system was used for HCA. HCA is a kind of cluster analysis method which aims to build a hierarchy of clusters in data mining and statistics.[34] In our experiments, the hierarchy is built from the individual cell by progressively merging clusters. We analyzed the spectral data in the region 550-1800 cm^{-1} and the data were vector normalized. Then we used Euclidean distance method and Ward's algorithm to calculate the spectral differences and form clusters.[26]

For PCA the same dataset with same pre-process was used. PCA was used to highlight the major variability existing in the spectral dataset. In this study, the PCA model was also calculated within the spectral region 550-1800 cm^{-1}. Then PCA was used to reduce the dimension of the dataset and the first 7 principal components (PCs) described 95.01% of the variance of the dataset.

SVM with a linear kernel was used to build a differentiation model for the four

different cell types. SVMs are a set of related methods for supervised learning, applicable to both classification and regression problems.[34] Here, all individual spectra from 200 cells (50 leukocytes, 50 H1299, 50 H460, and 50 A549) were background corrected using the daubechies wavelet transform (10 daubechies, 7 transform levels, 10 iterations) and vector normalized. SVM algorithm was trained and tested by using leave-one-out cross validation. This procedure was repeated with each omitted spectrum, discriminating each spectrum in turn. Finally, a probability of prediction was calculated and expressed as a sensitivity and specificity for each group. All 200 spectra could be classified correctly, giving a prediction accuracy of 100%.

3. Results and discussion

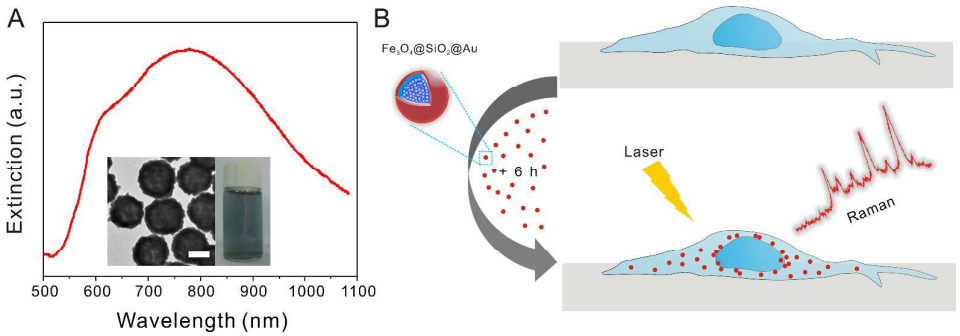

Figure 1 (A) Extinction spectrum of Au nanoshells (Fe_3O_4@SiO_2@Au) in water, and the insets show TEM image and optical image of Au nanoshells in water. The scale bar is 100 nm. (B) The general procedures for the preparation of cell samples and the SERS measurement of cells.

Figure 1A shows the extinction spectrum of Au nanoshells in aqueous solution with a strong and broad peak (dipolar resonance mode) centered at ~780 nm and a shoulder (quadrupolar resonance mode) at ~610 nm. The TEM image (inset in Figure 1A) shows that the average diameter of Au nanoshells is ~180 nm. The Au nanoshells

have shown the strong NIR SERS effect due to the large electric field enhancement at the dipolar plasmon resonance of the Au shells.[32] In our study, the cells were grown on quartz coverslips due to the low background interference. After the cells were grown to 80% confluence, they were incubated with Au nanoshells with a final concentration of 0.02 nM for six hours, and then the Raman measurements were taken (see Figure 1B). After the Au nanoshells are internalized by cells, they can greatly enhance the Raman signals of cell components near the shell surface. As various types of cells have different molecular compositions and structures, the SERS spectra can be used for distinguishing different cell types.[27, 28, 35]

Figure 2A shows the bright field images of representative examples of four types of cells (from top to bottom: H460, A549, H1299, and leukocytes) with SERS nanoprobes inside. In the bright field images, we could easily identify the nanoprobes with black colors in the cells. SERS nanoprobes were mainly located in the cytoplasm, and these results are consistent with previous reports about the cellular location of Au nanoparticles.[26, 36] Three closely related subtypes of NSCLC cells (H460, A549, and H1299) were adherent on the quartz coverslips, so they were slightly stretched. As leukocytes can't adhere to the coverslips, they were directly dropped onto the coverslip and appeared more or less round. On average the leukocytes are slightly smaller in size than the other cells. However, cancer cells have large heterogeneity including both size and morphology, and they are not universally larger than all leukocytes.[37, 38] Besides that, cells in blood are all suspended and their size difference will become smaller, therefore the size is not a reliable criterion used for

classification.[38]

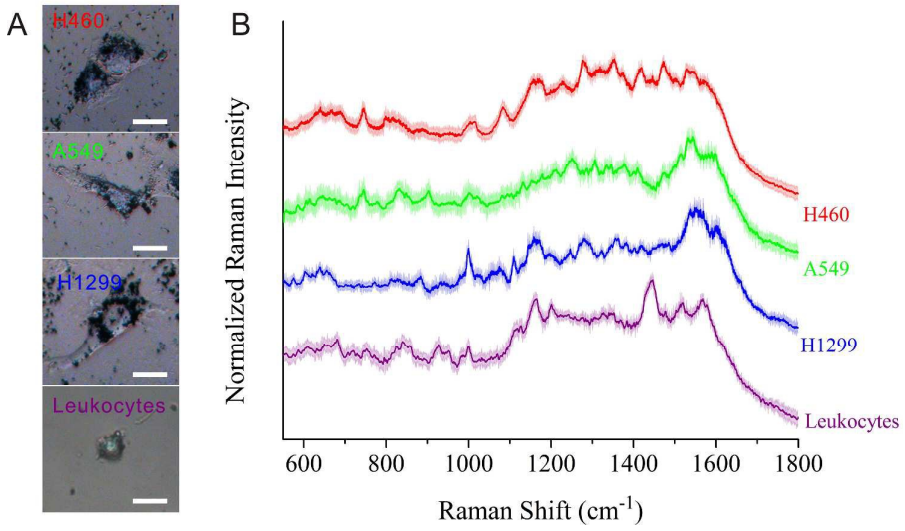

Figure 2 Bright-field images (A), and averaged and normalized SERS spectra (B) of four different types of cells (from top to bottom: H460, A549, H1299, leukocytes). The shaded areas represent the standard deviations of the means. SERS spectra were obtained from 550 to 1800 cm^{-1}. All scale bars in the bright-field images are 50 μm.

Averaged SERS spectra of four types of cells are depicted in Figure 2B. The shaded areas represent the standard deviations of the means. The SERS spectra were obtained with lower laser power (4.5 mW) and shorter integration time (3s) compared with normal Raman measurements.[30] This can greatly reduce the photo-damage of cells, so that the constituents and viabilities of native cells themselves can remain almost unchanged.[17] Therefore SERS has great potential to be used in live cell analysis. In this study, SERS spectra derived from specific cells were used to characterize the cellular biochemical composition of each individual type. 200 individual cells of four different types (50 H460, 50 A549, 50 H1299, 50 leukocytes) were tested and all SERS spectra were used for further statistical analysis. For the sake of convenient comparison, the intensity of the averaged SERS spectra for various types of cell was

normalized to obtain the relative intensity from 0 to 1 [10]. The Raman spectra of the cells can act as molecular fingerprints containing information from various cellular components such as DNA, protein, lipids and carbohydrates.[39] Molecular components of cells are very complex,[21] and typical molecules of interest are often associated with RNA, DNA, carbohydrates, proteins, or lipids. With the help of SERS probes, these biochemical molecules may typically be assessed based on their individual Raman band assignments. By reference to the SERS band assignments in previous reports,[10, 26, 40], we assigned the observed SERS bands in Table 1. The bands at around 747 cm^{-1} (T), 833 cm^{-1} (O-P-O backbone stretching), 1342 cm^{-1} (A, G), 1582 cm^{-1} (G, A) are assigned to nucleic acids. The bands at around 645 cm^{-1} (C-C twist in tyrosine), 833 cm^{-1} (tyrosine), 1002 cm^{-1} (phenylalanine), 1158 cm^{-1} (C–C and C-N stretch), 1252 cm^{-1} (amide III), 1307 cm^{-1} (C-N stretch), 1342 cm^{-1} (C-H deformation), 1414 cm^{-1} (aspartate and glutamate), 1543 cm^{-1} (tryptophan) are assigned to proteins and amino acids. And the band at around 1252 cm^{-1} (=CH deformation) is assigned to lipids. Although the SERS spectra of different types of cells look very alike at sometimes, they still have differences on some peak positions and peak intensities. In order to better compare and distinguish them, multivariate statistical methods including HCA, PCA and SVM were carried out.

Table 1 Assignment of the observed SERS bands based on the literature.[10, 26, 40]

Raman shift (cm^{-1})	Nucleic acid	Protein	Lipids
645		Tyrosine (C-C twist)	
747	T		
833	O–P–O str DNAbk	Tyrosine	
1002		Phenylalanine	
1158		C–C str (and C–N str)	
1252		amide III	=CH def
1307		C-N str	
1342	A, G	C-H def	
1414		Aspartate, Glutamate	
1543		Tryptophan	
1582	G, A		

str, stretching; def, deformation; bk, backbone.

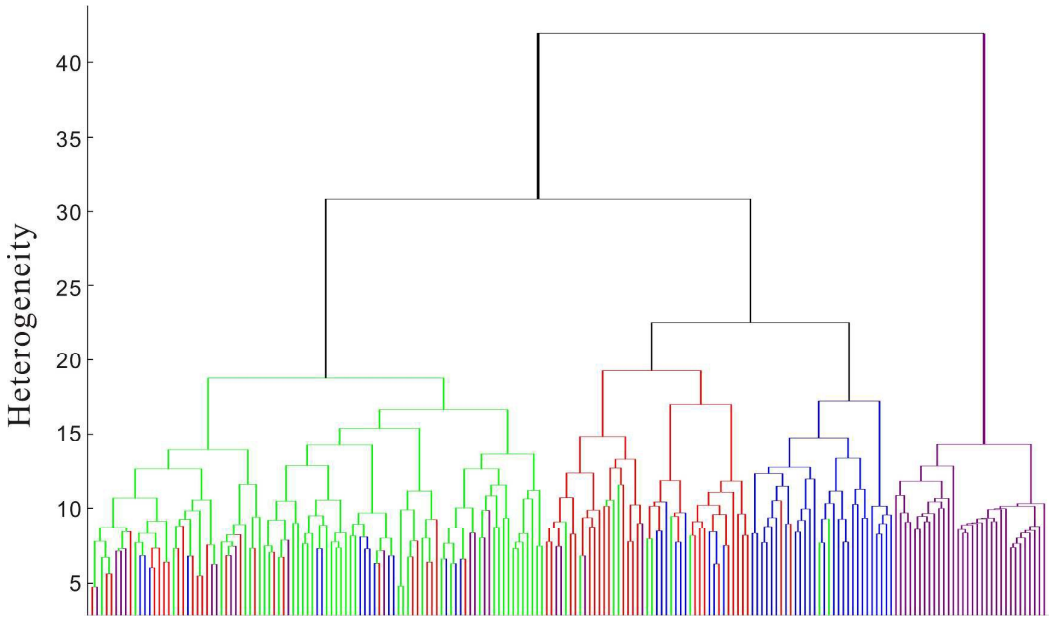

Figure 3 Dendrogram from the hierarchical cluster analysis in the spectral region from 550 to 1800 cm^{-1} of different types of cells is shown (leukocytes: purple, H460: red, A549: green and H1299: blue).

HCA is a kind of cluster analysis method which aims to build a hierarchy of clusters in data mining and statistics,[34] and this method has been successfully used in

identification and differentiation of breast cancer cells, leukaemia cells and leukocytes with normal Raman measurements.[26] In our study, HCA method was also used to form clusters according to the cell type. Euclidean distance method and Ward's algorithm were used to perform HCA and the spectra in the region 550-1800 cm^{-1} were vector normalized and averaged.[26] Figure 3 shows the dendrogram for all 200 cells. And we can see two well-separated major clusters: one for leukocytes and one for NSCLC cells. Within the NSCLC cell cluster, each cell type forms its own sub-cluster with some misclassifications. We can conclude from the dendogram that although vast majority of leukocytes were well separated, there were some misclassifications among the NSCLC cells. So the clustering result from the HCA can only separate leukocytes from lung cancer cells but cannot distinguish different lung cancer cells well because they are too closely related. The clustering result is similar to the previous study about lung cancer diagnosing.[41] In that study, two large clusters were clearly visible in the dendrogram, but no sub-clustering was evident for different subtypes of lung cancer cells and even no cluster patterns emerged. The possible reasons are small number of samples and great similarity between the samples.[41] Thus we speculate that HCA can achieve good results when distinguishing samples without high similarity, but several misclassifications may occur when distinguishing closely similar samples.

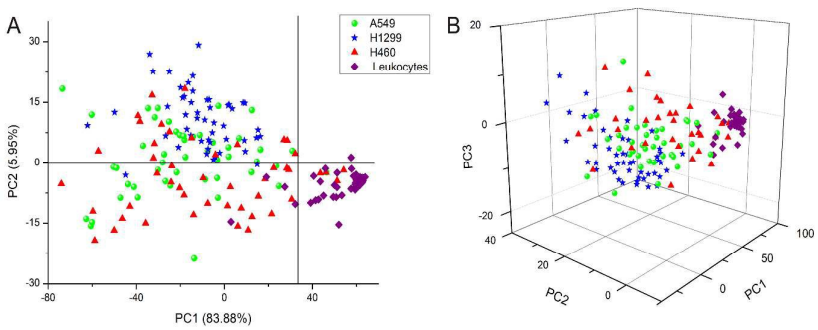

Figure 4 Principal component analysis (PCA) of four types of cells. PCA scores are analyzed and plotted in the spectral region of 550-1800 cm^{-1}. Each spot represents one cell and each cell type is coded by different colors and shapes.

Next, we employed the PCA method to evaluate the possibility of distinguishing different types of NSCLC cells and leukocytes. PCA can select less number of significant components through linear transformation of multiple variables. As a classic analysis method, PCA has been widely used in multivariate statistical analysis for spectra.[42, 43] Herein, the spectral differences in the data sets comprising 200 spectra of four types of cells within the same spectral region from 550 to 1800 cm^{-1} (consisting of 1910 data points) were analyzed by PCA. First, we can roughly distinguish three types of cells (H1299, H460, leukocytes) using the PCA method with some overlaps between the H460 and leukocytes (see Figure S1). Figure S1 shows the three-dimensional plot using the first, second and third principal components (PC1, PC2, and PC3). Different cell types are approximately separated as indicated by spectra assemblies with different colors and shapes. However, when it turned to four types of cells (A549, H1299, H460, leukocytes) that the distinguish effect became much worse (Figure 4). In Figure 4, using principal component scores PC1 (83.88% variation), PC2 (5.95% variation) and PC3 (1.83% variation), the scatter plots of

SERS spectra for each cell line were projected into the two-dimensional and three-dimensional images. We can see that the SERS spectra are mainly divided into two groups, one is leukocytes and the other is NSCLC cells, which is caused by the intrinsic difference in biomolecular composition and concentration between normal and cancer cells. This result is consistent with the clustering result from the HCA as shown in Figure 3. However, the plots groups of NSCLC cells are adjacent to each other and some even were overlapped with each other, which means they cannot be separated well. This result is similar to the previous studies.[26, 31] In those studies, PCA only separated normal cells from tumor cells but did not distinguish different tumor cells well. That means on high dimensional data of complex samples, especially when more samples are involved and the data have ambiguous distribution of noise features, PCA often cannot achieve good separation results.[43]

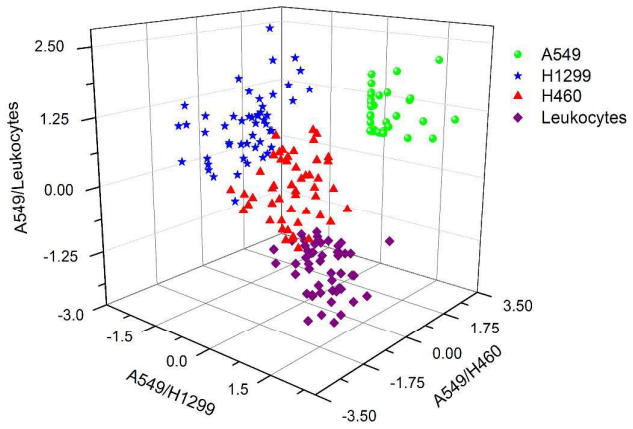

Figure 5 Graphical representation of the support vector machines with linear kernel for classification of four cell types. Three out of six decision values are plotted.

After the failure to discriminate subtypes of NSCLC cells using HCA and PCA method, SVM with a linear kernel were fed with this SERS dataset to create a

classification model in order to find a more suitable classification method. Figure 5 shows the analysis result using three out of the six decision values. It can be seen that four cell types are successfully separated as indicated by spectra assemblies with different colors and shapes. 200 spectra were used to train the SVM model with leave-one-out cross validation and all spectra could be classified correctly, giving an overall accuracy of 100% on a single-cell level. The details of the prediction accuracy of the classification model are presented in Table S1.

Although the SVM model with 100% accuracy was built, these cells were all involved in building this model. It will be more practical if this model can predict some "unknown" cells which were not involved in building this model but within these four cell types. To further demonstrate the accuracy and practicability of this SVM model, this trained and validated SVM model was used to predict and classify a test set (including additional 80 cells: 20 A549, 20 H1299, 20 H460, 20 leukocytes). It should be mentioned that none of the cells was included in building the SVM model. The detailed predicted results for the individual cell types are shown in Table 2. A predicted accuracy of 88.75% can be achieved on a single-cell level. If we want a better distinguish effect, more samples are needed both for training and testing the model.[44] For clinical purpose, the most relevant question is to identify the cancer cells from body's own healthy leukocytes.[45] For this purpose the SVM model trained with spectra showed very good characteristics: all NSCLC cells were correctly identified as cancer cells with 100% accuracy.

Table 2 Confusion table for the predicted result of 80 cells using the SVM model.

		Predicted labels			
		Leukocytes	A549	H1299	H460
True labels	Leukocytes	18	0	0	2
	A549	0	18	0	2
	H1299	0	2	18	0
	H460	0	2	1	17

We further evaluated the performance of this SVM model when there were more than 1 subtype of NSCLC cells in the sample. The mixtures of two subtypes of NSCLC cell (A549 and H1299) with different ratios were used as the test sets. It should be emphasized again that none of these cells was included in building the SVM model. Although fluorescent biomarkers can help to distinguish cells in the mixture, they may also produce strong Raman background in the SERS measurements. In order to verify the accuracy of the SVM model in mixed samples, we mixed SERS probes labeled A549 and blank H1299 at different ratios, thus we can recognize the cell type directly from the bright-field images.

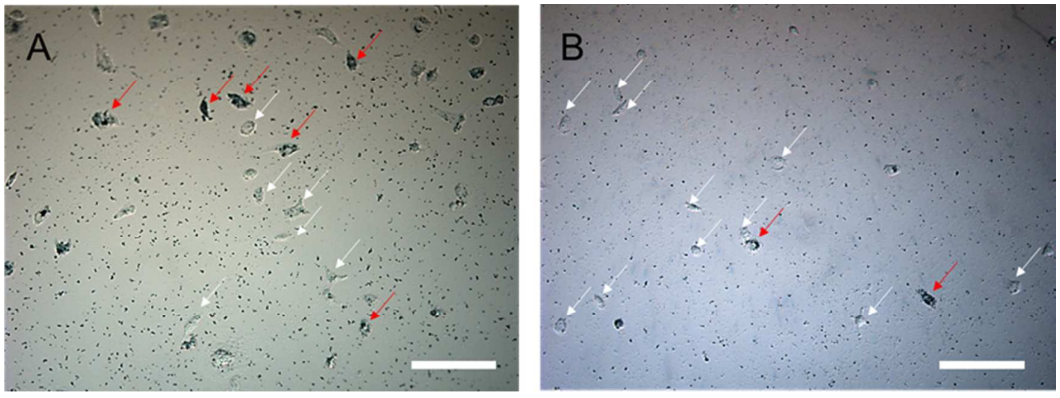

Figure 6 Bright-field images of the mixed two subtypes of NSCLC cells cultured on quartz coverslips. The ratio of A549: H1299 was (A) 1:1 and (B) 1:9. All scale bars are 200 μm.

Figure 6 shows the bright-field images from the mixtures of two subtypes of cell, where A549 can be recognized by SERS probes in the cells. Figure 6A represents the group in which A549 and H1299 were mixed at a ratio of 1:1 (A549 indicated by red arrows and H1299 by white arrows). Since the normal Raman signals of H1299 cells (no SERS probes inside) were very weak, we only detect the signal of A549 cells in mixed samples. Table 3A showed the predicted results based on the SVM model and an accuracy of 95% can be achieved on a single-cell level. Figure 6B represents the group in which A549 and H1299 were mixed at a ratio of 1:9, and a prediction accuracy of 100% can be achieved for A549 on a single-cell level (Table 3B). These results indicate the SVM model significantly improves the accuracy of prediction and classification of subtype of NSCLC cells in contrast to the HCA and PCA analysis methods.

Table 3. Confusion table for the mixed cell samples of A549:H1299 at the ratio of (A) 1:1 and (B) 1:9 using the SVM model.

A

		Predicted labels	
		A549	H1299
True labels	A549	19	1

B

		Predicted labels	
		A549	H1299
True labels	A549	5	0

4 Conclusions

In this study, we have used SERS spectroscopy and multivariate statistical methods including HCA, PCA and SVM to identify and distinguish three subtypes of NSCLC

cells and leukocytes on the single-cell level. With the help of statistical methods, a reproducible SVM model has been developed showing a much better classification performance compared to HCA and PCA method. The SVM classification model provides a predication accuracy of 88.75% for "unknown" independent cell types and an accuracy of ~95% for the mixed samples on a single-cell level. This predication accuracy can be further improved by using larger amount of samples to train the model. The fast identification of subtype of NSCLC cells by SERS spectra with multivariate analysis can assist doctors to choose appropriate treatment plans for lung cancer patients as soon as possible. This method could also be adapted to the detection and distinction of other types of cancer cell. Moreover, the SERS nanoprobes used in this work are composed of superparamagnetic cores, which potentially further allows the isolation and enrichment of cancer cells in peripheral blood. We believe that future promising work may involve SERS and magnetic separation method combined with multivariate analysis as a rapid, simple, non-destructive and accurate diagnostic tool in early stage cancer detection and cancer-therapy monitoring.

Associated content

Supporting Information

This information is available free of charge via the internet.

Acknowledgements

We gratefully acknowledge the National Natural Science Foundation of China (No. 81571763 and 21375087), the Science and Technology Commission of Shanghai

Municipality (No. 13ZR1422100) and Shanghai Jiao Tong University (No. YG2014MS53 and SJTU-KUL Bilateral Program) for their financial support. C.H. thanks the financial support of the Presidential Foundation of IMECAS.

References

1. *International Agency for Research on Cancer. Cancer Research UK (2012). World cancer factsheet*, Cancer Research UK: London, 2012.
2. L. G. Collins, C. Haines, R. Perkel and R. E. Enck, *Am Fam Physician*, 2007, **75**, 56-63.
3. I. Petersen and S. Petersen, *Anal. Cell. Pathol.*, 2001, **22**, 111-121.
4. L. Wang, T. Guo, Q. Lu, X. Yan, D. Zhong, Z. Zhang, Y. Ni, Y. Han, D. Cui, X. Li and L. Huang, *ACS Appl. Mater. Interfaces*, 2015, **7**, 359-369.
5. T. Hensing, A. Chawla, R. Batra and R. Salgia, in *Systems Analysis of Human Multigene Disorders*, eds. N. Maltsev, A. Rzhetsky and T. C. Gilliam, Springer New York, 2014, ch. 5, pp. 85-117.
6. J.-E. C. Holty, W. G. Kuschner and M. K. Gould, *Thorax*, 2005, **60**, 949-955.
7. C. Alix-Panabieres and K. Pantel, *Lab on a Chip*, 2014, **14**, 57-62.
8. S. Bhana, Y. Wang and X. Huang, *Nanomedicine*, 2015, **10**, 1973-1990.
9. Z. A. Nima, M. Mahmood, Y. Xu, T. Mustafa, F. Watanabe, D. A. Nedosekin, M. A. Juratli, T. Fahmi, E. I. Galanzha and J. P. Nolan, *Scientific reports*, 2014, **4**.
10. C. Shi, X. Cao, X. Chen, Z. Sun, Z. Xiang, H. Zhao, W. Qian and X. Han, *Biomaterials*, 2015, **58**, 10-25.
11. J. Ye, F. Wen, H. Sobhani, J. B. Lassiter, P. V. Dorpe, P. Nordlander and N. J. Halas, *Nano Lett.*, 2012, **12**, 1660-1667.
12. J. F. Li, Y. F. Huang, Y. Ding, Z. L. Yang, S. B. Li, X. S. Zhou, F. R. Fan, W. Zhang, Z. Y. Zhou, Y. WuDe, B. Ren, Z. L. Wang and Z. Q. Tian, *Nature*, 2010, **464**, 392-395.
13. A. Wang, W. Ruan, W. Song, L. Chen, B. Zhao, Y. M. Jung and X. Wang, *J. Raman Spectrosc.*, 2013, **44**, 1649-1653.
14. Y. Zhang, S. Liu, L. Wang, X. Qin, J. Tian, W. Lu, G. Chang and X. Sun, *RSC Adv.*, 2012, **2**, 538-545.
15. M. Wang, X. Cao, W. Lu, L. Tao, H. Zhao, Y. Wang, M. Guo, J. Dong and W. Qian, *RSC Adv.*, 2014, **4**, 64225-64234.
16. S. Nie and S. R. Emory, *Science*, 1997, **275**, 1102-1106.
17. K. Kneipp, A. S. Haka, H. Kneipp, K. Badizadegan, N. Yoshizawa, C. Boone, K. E. Shafer-Peltier, J. T. Motz, R. R. Dasari and M. S. Feld, *Appl. Spectrosc.*, 2002, **56**, 150-154.
18. J. L. Deng, Q. Wei, M. H. Zhang, Y. Z. Wang and Y. Q. Li, *J. Raman Spectrosc.*, 2005, **36**, 257-261.
19. S. Feng, D. Lin, J. Lin, B. Li, Z. Huang, G. Chen, W. Zhang, L. Wang, J. Pan and R. Chen, *Analyst*, 2013, **138**, 3967-3974.
20. S. Feng, R. Chen, J. Lin, J. Pan, Y. Wu, Y. Li, J. Chen and H. Zeng, *Biosens. Bioelectron.*, 2011, **26**, 3167-3174.
21. H. Huang, W. Chen, J. Pan, Q. Chen, S. Feng, Y. Yu, Y. Chen, Y. Su and R. Chen, *J. Spectrosc*,

2011, **26**, 187-194.

22. X. Wu, L. Luo, S. Yang, X. Ma, Y. Li, C. Dong, Y. Tian, L. e. Zhang, Z. Shen and A. Wu, *ACS Appl. Mater. Interfaces*, 2015, **7**, 9965-9971.
23. S. Feng, J. Lin, Z. Huang, G. Chen, W. Chen, Y. Wang, R. Chen and H. Zeng, *Appl. Phys. Lett.*, 2013, **102**, 043702.
24. M. J. Sailor and J. H. Park, *Adv. Mater.*, 2012, **24**, 3779-3802.
25. K. Galler, K. Brautigam, Gro, J. Popp and U. Neugebauer, *Analyst*, 2014, **139**, 1237-1273.
26. U. Neugebauer, J. H. Clement, T. Bocklitz, C. Krafft and J. Popp, *J. Biophotonics*, 2010, **3**, 579-587.
27. I. Notingher, G. Jell, P. L. Notingher, I. Bisson, O. Tsigkou, J. M. Polak, M. M. Stevens and L. L. Hench, *J. Mol. Struct*, 2005, **744–747**, 179-185.
28. T. Bocklitz, M. Putsche, C. Stüber, J. Käs, A. Niendorf, P. Rösch and J. Popp, *J. Raman Spectrosc.*, 2009, **40**, 1759-1765.
29. E. Ly, O. Piot, A. Durlach, P. Bernard and M. Manfait, *Analyst*, 2009, **134**, 1208-1214.
30. A. Huefner, W.-L. Kuan, R. A. Barker and S. Mahajan, *Nano Lett.*, 2013, **13**, 2463-2470.
31. S. Mert and M. Çulha, *Appl. Spectrosc.*, 2014, **68**, 617-624.
32. X. Jin, H. Li, S. Wang, N. Kong, H. Xu, Q. Fu, H. Gu and J. Ye, *Nanoscale*, 2014, **6**, 14360-14370.
33. J. H. Clement, M. Schwalbe, N. Buske, K. Wagner, M. Schnabelrauch, P. Görnert, K. O. Kliche, K. Pachmann, W. Weitschies and K. Höffken, *J Cancer Res Clin Oncol*, 2006, **132**, 287-292.
34. O. Maimon and L. Rokach, *Data mining and knowledge discovery handbook*, Springer, 2005.
35. P. Rösch, M. Harz, M. Schmitt and J. Popp, *J. Raman Spectrosc.*, 2005, **36**, 377-379.
36. A. Shamsaie, M. Jonczyk, J. Sturgis, J. Paul Robinson and J. Irudayaraj, *J. Biomed. Opt.*, 2007, **12**, 020502.
37. S. Riethdorf, H. Fritsche, V. Müller, T. Rau, C. Schindlbeck, B. Rack, W. Janni, C. Coith, K. Beck, F. Jänicke, S. Jackson, T. Gornet, M. Cristofanilli and K. Pantel, *Clin Cancer Res*, 2007, **13**, 920-928.
38. W. Chen, S. Weng, F. Zhang, S. Allen, X. Li, L. Bao, R. H. W. Lam, J. A. Macoska, S. D. Merajver and J. Fu, *ACS Nano*, 2013, **7**, 566-575.
39. H. Yamakoshi, K. Dodo, M. Okada, J. Ando, A. Palonpon, K. Fujita, S. Kawata and M. Sodeoka, *J. Am. Chem. Soc.*, 2011, **133**, 6102-6105.
40. P. Lu, J. Wang, J. Lin, J. Lin, N. Liu, Z. Huang, B. Li, H. Zeng and R. Chen, *J. Biomed. Opt.*, 2014, **20**, 051005.
41. P. Lewis, K. Lewis, R. Ghosal, S. Bayliss, A. Lloyd, J. Wills, R. Godfrey, P. Kloer and L. Mur, *BMC Cancer*, 2010, **10**, 640.
42. U. Thissen, M. Pepers, B. Üstün, W. J. Melssen and L. M. C. Buydens, *Chemometr. Intell. Lab.*, 2004, **73**, 169-179.
43. C. Hu, J. Wang, C. Zheng, S. Xu, H. Zhang, Y. Liang, L. Bi, Z. Fan, B. Han and W. Xu, *Med. Phys.*, 2013, **40**, 063501.
44. C. Beleites, U. Neugebauer, T. Bocklitz, C. Krafft and J. Popp, *Anal. Chim. Acta*, 2013, **760**, 25-33.
45. U. Neugebauer, C. Kurz, T. Bocklitz, T. Berger, T. Velten, J. Clement, C. Krafft and J. Popp, *Micromachines*, 2014, **5**, 204-215.